Composite Structures 290 (2022) 115544

Contents lists available at ScienceDirect

Composite Structures

journal homepage: www.elsevier.com/locate/compstruct

Structural analysis for the design of a lightweight composite railway axle

M.S. Johnson [a], R. Evans [a], P.J. Mistry [a,*], S. Li [a], S. Bruni [b], A. Bernasconi [b], S. Cervello [c]

[a] Composites Research Group, Faculty of Engineering, University of Nottingham, Advanced Manufacturing Building, Jubilee Campus, NG8 1BB, UK
[b] Department of Mechanical Engineering, Politecnico di Milano, Italy
[c] Lucchini R.S. SpA, Lovere, Italy

ARTICLE INFO

Keywords:
Railway axle
Lightweighting
Unsprung mass
Composite material
NEXTGEAR
Structural analysis

ABSTRACT

The unsprung masses associated with the axles of a railway vehicle result in costly impact damage to the rail infrastructure. A hybrid metallic-composite (HMC) railway axle is evaluated using finite element analysis. The axle mass is 74 kg, 63% lighter than an equivalent hollow steel axle. The HMC railway axle comprises a full length, carbon fibre reinforced, epoxy matrix composite tube with secondary overwrapping for stiffness and EA1N grade steel collars creating the wheel seats and journal surfaces. Maximum axle deflection is 1.72 mm with a misalignment at the journals of 0.21°, potentially requiring a bearing reassessment. Nominal bending stress in the axle is 99.3 MPa (Tsai-Wu damage index of 0.18). Peak bending and torsional stresses result in Tsai-Wu damage indexes of 0.71 and 0.42, respectively. The methodology in this paper can be extended to the design of future lightweight composite shafts to benefit many other industries.

1. Introduction

The European rail infrastructure is used intensively with the trend towards additional increases in the future [1]. Exploitation of short range and urban railway lines is particularly acute with commuter rail, metro lines and tram/light rail usage totalling nearly 27 billion passengers per year [2]. Increased usage of the of the rail infrastructure leads to track degradation, impacting on maintenance costs and usage availability. While it is critical to design track systems that are less subject to damage and degradation, the new generation of rolling stock must be engineered to substantially reduce damage to the infrastructure. Dynamic effects caused by the sprung masses, bogies and car bodies, can be mitigated by vehicle suspensions. However, the dynamic loads arising from the unsprung masses cannot be reduced since these bodies are in direct contact with the track. The unsprung masses include the wheelsets comprising the wheels, bearings and in some cases brake disks, all fitted to a common axle. Dynamic forces caused by the unsprung masses largely are responsible for damage phenomena including irregular track settlement, rolling contact fatigue and corrugation of the rails [3]. Therefore, lightweighting of the unsprung masses is critical for extending the life of track components, reducing track maintenance costs and increasing the availability of the infrastructure.

Modern wheelsets are made entirely of standardised steels having the advantage of well characterised material properties with treatments known to enhance fatigue reliability [4,5]. Centre boring is the current practice for reducing the mass of steel railway axles with assurances of safety being maintained. To provide a further step-change in railway axle mass reduction, material substitution is necessary [6] which must be balanced against the need to maintain axle fatigue reliability. Ultimately, probabilistic fatigue assessment techniques as presented by notable authors [7–9] need to be applied to these new material solutions, providing continuity in safety and reliability.

The European Union (EU) funded project NEXTGEAR targets the use of new materials and mechatronic technologies for the design of robust and sustainable railway vehicles. Within Work Package (WP) 3 of this project, "The wheelset of the future," a lightweight, hybrid metallic-composite (HMC) railway axle was proposed, see Mistry et al. [10]. Prior to this, only one other composite railway axle has been identified for use on the British Rail, Advanced Passenger Train in the early 1980's [11]. While this example was a success from a structural and mass savings perspective, higher order design requirements, particularly damage tolerance, were not addressed. The solution by Mistry et al. advanced the state of art in railway axles by proposing a full length, primary composite tube (carbon fibre/epoxy) with a central, secondary composite tube (carbon fibre/epoxy) and bonded titanium collars at each end. This design was supported by a parametric study defining realistic dimensions for the HMC railway axle. Importantly, the axle had an approximate mass of 50 kg compared to an equivalent hollow steel railway axle with a mass of 198 kg.

* Corresponding author.
E-mail address: preetum.mistry@nottingham.ac.uk (P.J. Mistry).

https://doi.org/10.1016/j.compstruct.2022.115544
Received 3 November 2021; Received in revised form 1 March 2022; Accepted 1 April 2022
Available online 6 April 2022

Nomenclature

a	Distance between running surface and loading plane (mm)
$d_{o,c}, d_{o,p}, d_{o,s}$	Outer diameter of the metallic collar, primary composite tube and secondary composite tube, respectively (mm)
$d_{i,c}, d_{i,p}, d_{i,s}$	Inner diameter of the metallic collar, primary composite tube and secondary composite tube, respectively (mm)
$F'_{f,x}$	Vertical brake force (N)
F'_{y}	Tangential brake force (N)
$F'_{f,z}$	Horizontal brake force (N)
L	Distance between running surfaces (mm)
L_{ω}	Distance between loading planes (mm)
l_c, l_p, l_s	Length of metallic collar, primary composite tube and secondary composite tube, respectively (mm)
M	Bending moment (General) (Nmm)
M_x	Bending moment about x-axis due to static vertical force (Nmm)
M'_x	Bending moment about the x-axis due to vertical braking (Nmm)
My'	Torsional moment about the y-axis (Nmm)
M'_z	Bending moment about the z-axis due to horizontal braking (Nmm)
m_c^{EA1N}, m_p, m_s	Mass of metallic collar, primary composite tube and secondary composite tube, respectively (kg)
P_x	Static vertical force on the journal due to vehicle mass (N)
P'_x	Reacting vertical brake force at journal (N)
P'_z	Reacting horizontal brake force at journal (N)
Q_x	Reacting vertical force on the wheel due to vehicle mass (N)
t_c, t_p, t_s	Thickness of the metallic collar, primary composite tube and secondary composite tube respectively (mm)
u_x, u_y, u_z	Displacement in the $\times$, y and z directions, respectively (mm)
u_{rx}, u_{ry}, u_{rz}	Rotation about the $\times$, y and z axes, respectively (°)
V	Shear force (General) (N)
V_x	Vertical shear force due to vehicle mass (N)
V'_x	Shear force due to vertical braking (N)
V'_y	Shear force due to tangential braking (N)
V'_z	Shear force due to horizontal braking (N)
ΔL_{BtB}	Change in back-to-back distance between wheels at rail level (mm)
δ_{max}	Maximum deflection at centre of axle (mm)
θ_{max}	Maximum rotation at bearing (°)
σ_B	Bending stress (General) (MPa)
τ_{horiz}	Maximum horizontal (transverse) shear stress (MPa)
$\tau_{torsion}$	Torsional shear stress (MPa)
φ	Angle of twist of axle between running surfaces (°)
ω_1	First critical speed of axle between loading planes (Hz)

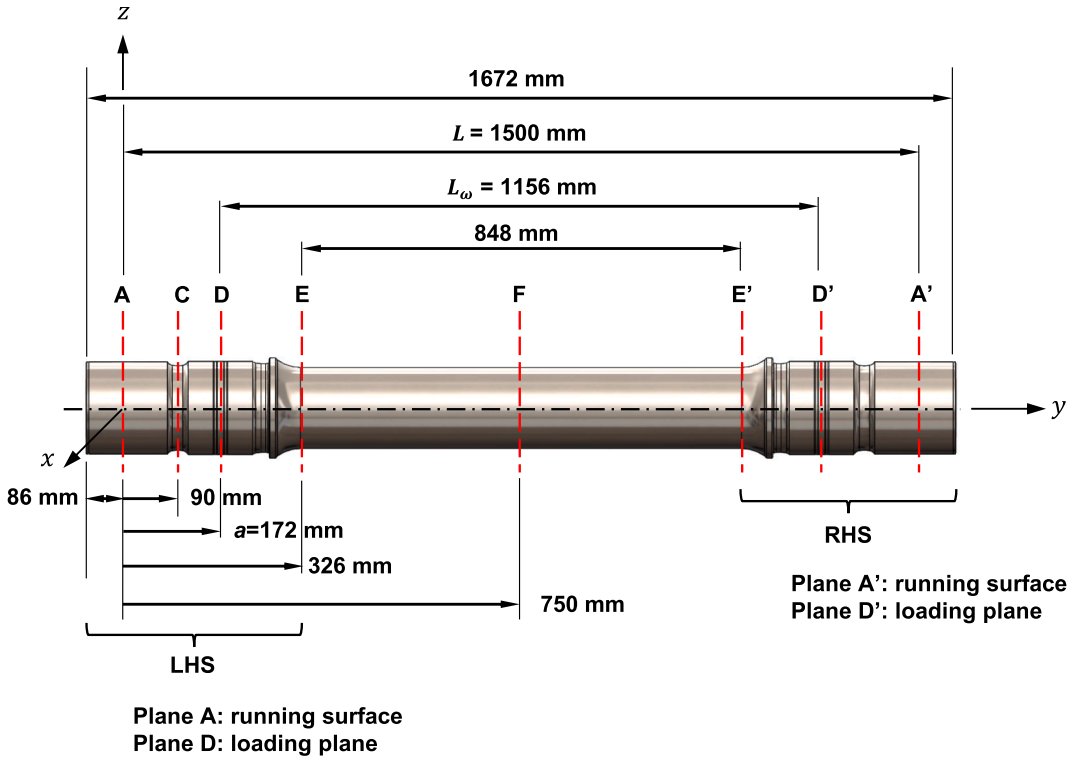

Fig. 1. Inboard bearing, hollow trailer axle as manufactured by Lucchini R.S. showing positions of the critical sections along the length.

This paper improves upon that work in the following ways:

- A finite element (FE) model is used to provide a preliminary structural assessment of performance of the proposed HMC axle under loading.
- The loading to the axle is applied as individual forces to produce moments rather than being applied as a single, resultant moment (MR) as specified within railway axle standard, Standard BS 8535 [12].

It is recognised that a railway axle is a complex, safety critical

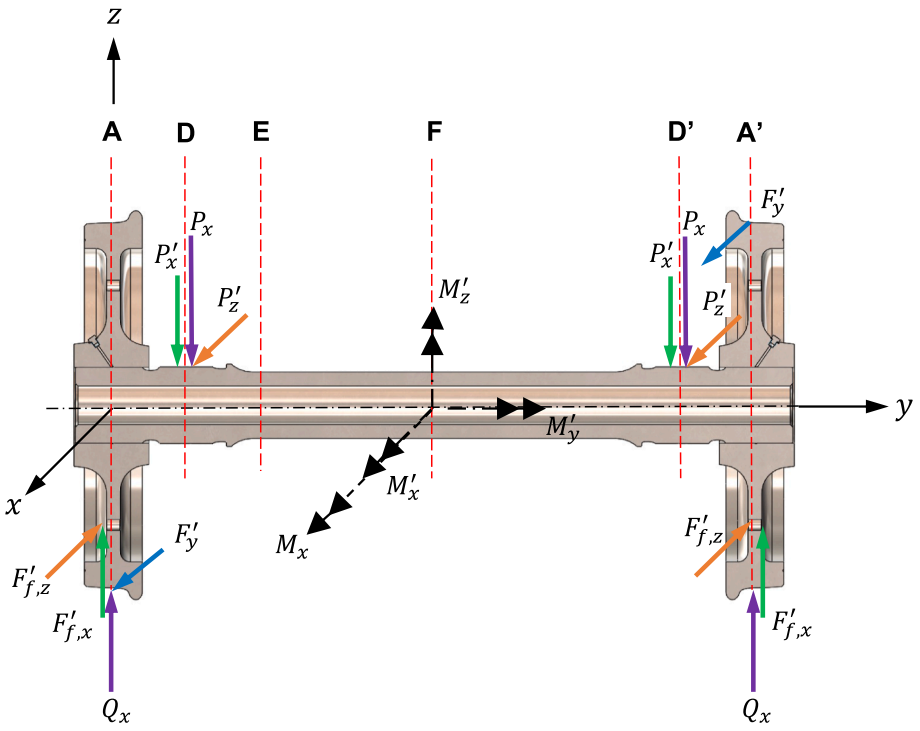

Fig. 2. Inboard bearing, wheelset assembly showing the global coordinate system and loads as used for the HMC railway axle analysis. The sense of the *y* and *z*-axes are transposed compared to the Standard [12].

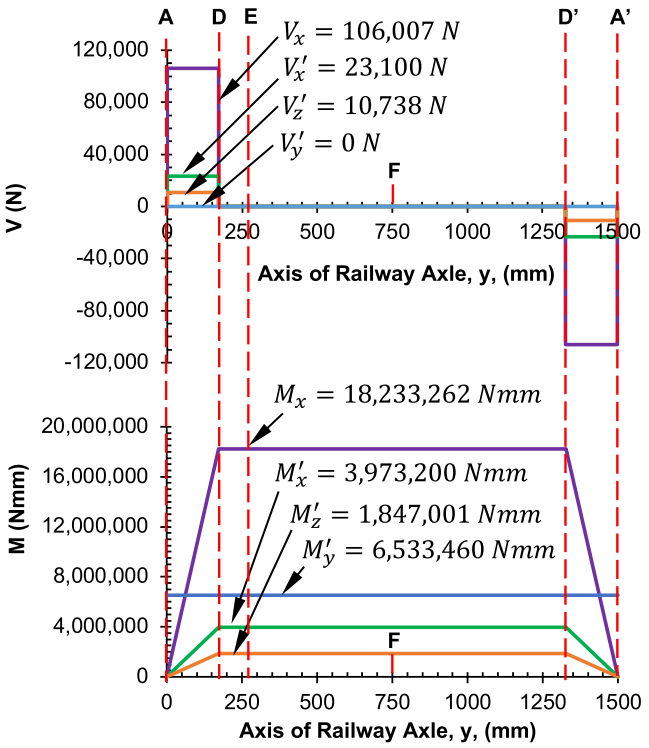

Fig. 3. Shear and bending moment diagrams for the railway axle subjected to moments, as provided by Lucchini R.S. [16].

component subject to stringent requirements. While fatigue performance is inextricable from the design of the primary structure, other functions such as damage tolerance and fire performance may be addressed as independent solutions. For clarity, the scope of this paper is restricted to a structural analysis of a lightweight composite railway axle. The essential requirement is that the composite axle is lighter than a hollow steel axle under the same loading conditions set out in the Standard BS 8535.

While the analysis presented pertains to a highly loaded railway axle application, a generalised methodology is proposed which could be adopted for any composite shaft with attached elements. This is important for shafts used in power transmission, subject to radial loads, for example when gears are in mesh. Under these rotating bending loads, there are few examples of composite shafts as most applications found are for driveshafts under pure torsion [13–15]. Repeated application and removal of the torsional load, while a contributor to cyclic fatigue, is less demanding than that from fully reversed, rotating bending as is the case for a railway axle.

2. Railway axle load cases

The aim of this work is to establish that the composite railway axle is lighter than a hollow steel axle under the same loading conditions set out in the Standard BS 8535. This section first defines the hollow steel axle parameters, then describes the standard load cases to be applied.

An inboard bearing, hollow trailer axle as manufactured by Lucchini R.S. [16] is illustrated in Fig. 1. This includes the main linear dimensions and distances to critical sections on the axle.

A wheelset assembly including this axle is depicted in Fig. 2 with a global coordinate system. The *y*-axis is aligned with the rotating axis of the axle. The *x*-axis is in the direction of travel of the vehicle. The *xy*-plane is parallel to the ground. The *z*-axis is perpendicular to the *xy*-plane. There are three types of forces listed in the Standard [12] to be considered in the design of the railway axle as a function of:

1. The "masses in motion." This is that static weight of the rail vehicle, P_x (N), which operates in the vertical (z) direction through the journals (the loading planes, D and $D^{'}$). The reaction forces at the wheels, Q_x, act through the running surfaces (A and $A^{'}$). Q_x is used to calculate a bending moment about the x-axis, M_x (Nmm).

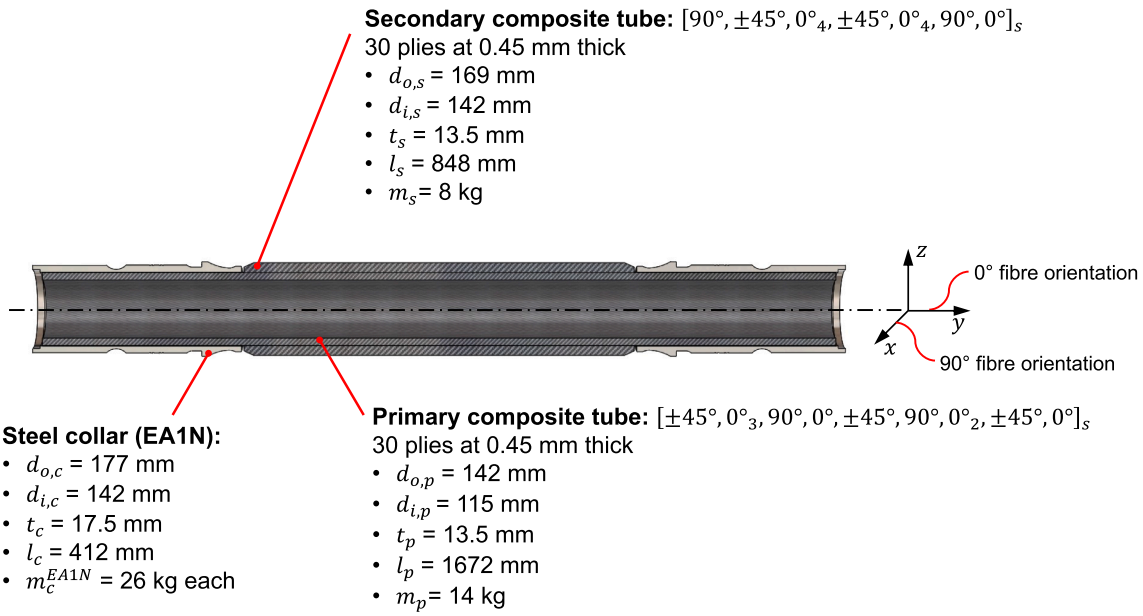

Fig. 4. Redesigned HMC railway axle comprising a full length, primary composite tube, a secondary composite tube and bonded steel collars.

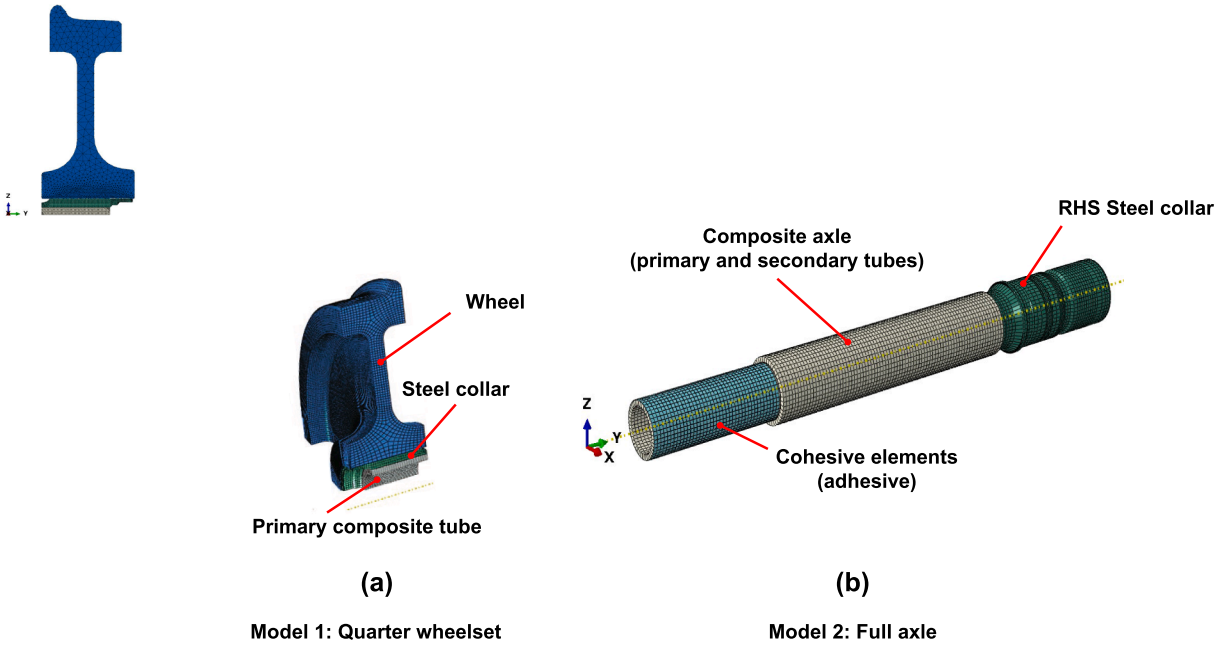

Fig. 5. HMC axle finite element mesh. (a) Model 1: Quarter wheelset, consisting of the primary composite tube, collar and wheel (adhesive layer is not visible). (b) Model 2: Full axle without wheels (LHS collar hidden to show cohesive elements beneath).

2. The braking system. In generalised form, a braking application generates moments represented by the three components $M_x^{'}$, $M_y^{'}$ and $M_z^{'}$ (Nmm). In the case of the trailer axle, the brake discs are mounted on the wheel web rather than along the axle and equal braking forces prevent a torsional moment to act around the axle centreline (*y*-axis). For completeness, an assumed moment, $M_y^{'}$, is included to account for a braking imbalance as well as effects due to curving and wheelset hunting. This is represented diagrammatically in Fig. 2 as $F_y^{'}$ (N) applied tangentially to the wheel, but is included as a pure moment at Position $D^{'}$ in the finite element models (Section 3.2). The frictional forces at the disc, $F_{f,x}^{'}$ (N) and $F_{f,z}^{'}$ (N) are transferred to the journal (Positions *D* and $D^{'}$), and represented as $P_x^{'}$ (N) and $P_z^{'}$ (N) to generate the respective braking moment components, $M_x^{'}$ and $M_z^{'}$. This permits use of realistic loading and boundary conditions in the FE models (Sections 3.2 and 3.3).
3. The traction. Power transmission generates forces leading to bending and torsion within the axle. According to the Standard [12], these are smaller than those generated due to braking and do not occur simultaneously with braking. The traction moments are not considered within this analysis as the trailer bogie is being considered.

The loads P_x, $P_x^{'}$ and $P_z^{'}$ produce bending and torsional moments, *M*, as well as internal shear forces, *V*, within the axle (Fig. 3). The value of the moments are taken from loading data supplied by Lucchini R.S. [16]. For simplicity these are represented as point loads and fixings, rather

than as distributed loads across the journal. As the axle is in four-point bending, there is zero shear force between the loading planes ($D - D'$). The maximum bending moment occurs between these loading planes and is constant. The torsional moment, M'_y, has no accompanying shear force. Position E is highlighted as the axle location with the smallest diameter and is regarded as a critical section. Position F, the centre of the axle, is where the maximum deflection occurs.

3. Modelling approach for the finite element analysis (FEA) of the HMC railway axle

The standard loads in Fig. 3 are applied to the redesigned HMC railway axle as adapted from the work of Mistry et al [10] and shown in Fig. 4.

The parametric study in that previous work was sufficient to size the axle diameters using a mechanics of materials approach coupled with a netting analysis to define the proportion of fibres orientated to align with the loading. However, the complexity of the composite axle with a total of 60 individual, unidirectional plies demanded use of an FE model (Fig. 5) for a more detailed assessment. Two configurations (Models 1 and 2) are necessary to analyse the different loading conditions. Due to the asymmetric nature of the material and out-of-plane loading, a three-dimensional model with continuum elements was developed rather than applying axisymmetric elements with asymmetric loading. The analysis is assessed at the mesoscale to obtain the stress distribution within each lamina. The laminate is defined by a stacking sequence, material type and lamina thickness.

Fig. 5a, Model 1, shows the axle configured as a quarter wheelset to simulate the interference fit between the wheel hub and collar. In Fig. 5b, the model is expanded to a full axle representation (Model 2), without the wheels, to simulate the global response of the axle subjected to bending and torsional loads.

To confirm the initial boundary conditions and application of loads, a beam element model (Model 3) also was used, in conjunction with the full axle model, comparing the observed displacements and nodal sectional forces. Once confirmed by Model 3, the Models 1 and 2 were used exclusively for the FE analysis.

The FE models are described in the following sections including the loading, boundary conditions and associated assumptions.

3.1. Description of the HMC railway axle models

The FE model of the HMC axle (Fig. 5) is meshed with the collar, tubes, adhesive (Model 2) and representative wheel (Model 1). The primary and secondary tubes of the axle are meshed using eight node, linear, continuum shell elements (SC8R). A single element is used for each angled ply with three material points through the thickness. Both tubes are defined as a laminate material section (UCHM450 SE 84LV) supplied by Gurit (Table A3) using Simpson's rule integration. Tube layups are reported in Fig. 4. The collars and wheel are modelled as eight node, linear solid elements (C3D8) using an isotropic material definition representing EA1N (Table A1) and ER7 (Table A2) steel, respectively. A single layer of cohesive elements (COH3D8), 0.2 mm thick, are positioned between the collar and tube to represent the structural adhesive supplied by 3 M™ (Table A4). An average element size of 5 and 10 mm is defined for all components of the HMC axle and wheel, respectively. To assess the damage allowable of the composite, the Tsai-Wu failure criterion [17] is implemented in Python [18] as a custom field-output.

The reference beam element model (Model 3) is represented using three node, quadratic elements (B32). The axle is defined as a thick-walled pipe cross section, with varying sectional and material properties along the length. The effective material properties of the composite tube are calculated by classical lamination theory (CLT) [19] for the layup, including the steel collar, to determine the sectional axial tensile stiffness across its length. The CLT approach, implemented in MATLAB [20], was also further verified within the FE model by assigning the constitutive matrices as a generalised shell stiffness to the tubes.

3.2. Loading conditions for the HMC railway axle models

The loads associated with the masses in motion and braking conditions are shown in Fig. 2 along with the moments generated (bending and torsional). For the wheelset model (Model 1), the loading is defined as an interference fit between the axle and the wheel hub. A nodal overlap of 0.3255 mm is applied representing the upper allowable dimensional tolerance [21]. The surface contact and interaction properties are defined between the wheel hub and collar edges to be finite-sliding, with a 'hard' contact-overclosure. The interaction tangential behaviour coefficient is given as 0.1.

For the full axle (Model 2), bending moments arise from loading at the axle journals, Positions D and D'. The static weight of the vehicle, P_x, and the representative vertical braking force, P'_x, provide bending around the $\times$ axis. Additional bending about the z axis develops from the representative braking force, P'_z. The braking forces are initiated at the brake discs, however, to maintain the boundary conditions (Section 3.3), these are transferred to the axle journals resulting in the equivalent bending and shear moments. These three forces are superimposed as the bending load case. The assumed torsional load is imposed as a pure moment, M'_y, at Position D'.

The loads, P_x, P'_x, and P'_z as well as the moment, M'_y, are applied to the element surface of the journal seats using an element to nodal coupling, located at the centre line point of each journal, where coordinates $x = z = 0$. The same loading approach is adopted for the beam element model (Model 3).

3.3. Boundary conditions for the HMC railway axle models

Finite element boundary conditions are defined for each model. For the quarter wheelset model (Model 1), symmetry conditions are defined in the x and z axis as $u_x = u_{ry} = u_{rz} = 0$ and $u_z = u_{rx} = u_{ry} = 0$, respectively. For clarification, "u_x" represents translation in the $\times$ direction and "u_{ry}" denotes rotation about the y axis with the other subscripts following the same logical format. For the full axle element model (Model 2), the boundary conditions are defined for the axle without wheels. These are imposed on the wheel hub element surface using an element to nodal coupling. This applies for the translational degrees of freedom (DOF) between the external nodes of the seat surface and a reference node. The reference node is located at the centre axis of the wheel seat, where coordinates $x = z = 0$, constrained as $u_x = u_y = u_z = u_{ry} = 0$ at Position A and $u_x = u_z = 0$ at Position A'. The same boundary conditions and approach are adopted for the beam element model (Model 3).

3.4. Assumptions for the FEA modelling of the HMC railway axle

Several assumptions are made in the analysis of the HMC railway axle, which include:

- The analysis is assumed to be a quasi-static, linear elastic analysis, conducted at the mesoscale. No dynamic or vibrational effects are considered.
- The primary and secondary composite tubes are to be manufacture by co-curing and considered as one component, with individual material properties.
- While a 0.2 mm adhesive layer is included within the model, the cohesive stress results are not considered.
- For the bending and torsional analyses, a high-cycle (10^7) fatigue safety factor of 0.5 is applied, reducing the ultimate strength of the materials [22]. For clarity, fatigue properties are not used in Model 1 for assessing the interference fit between the wheel hub and collar.

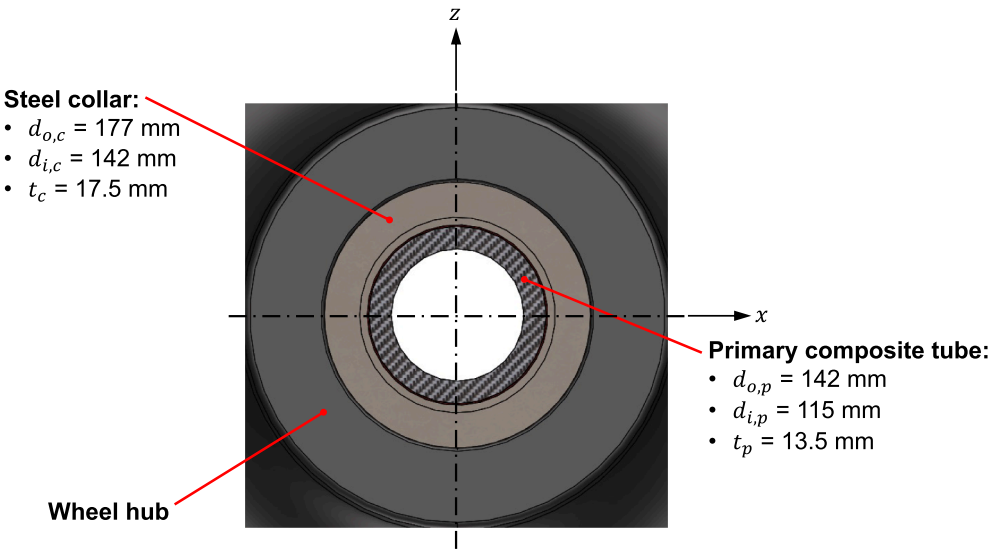

Fig. 6. Cross section through the HMC axle and wheel hub at the running surface (Position *A*) showing the diameters of the metallic collar and the primary composite tube.

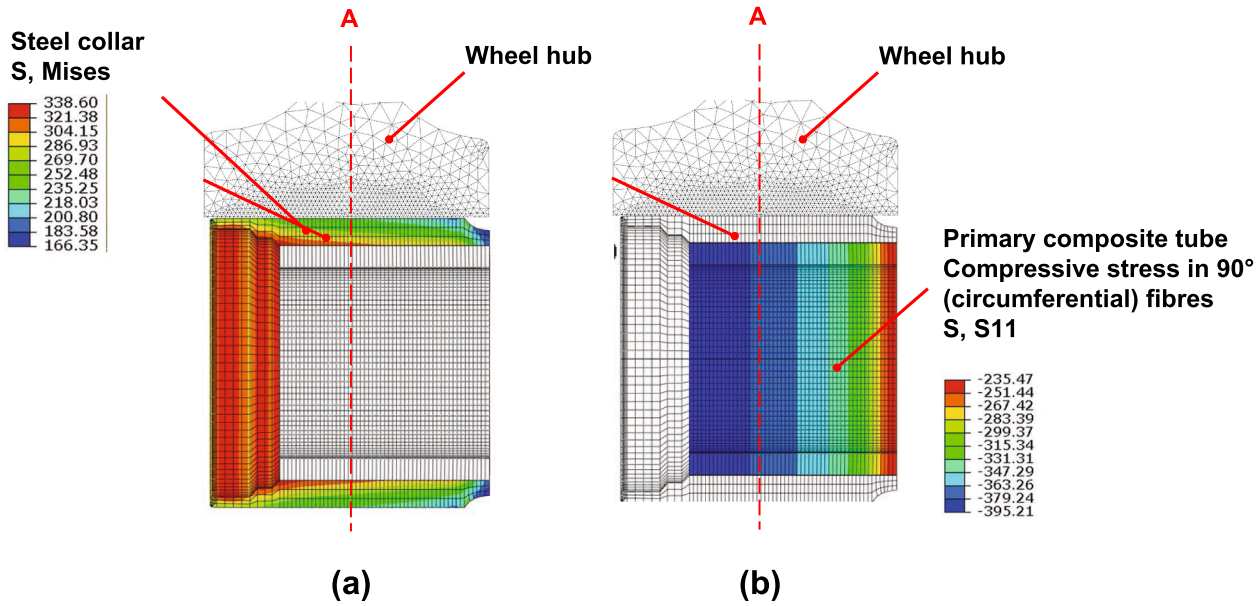

Fig. 7. Stress fields at Position *A* from the interference fit between the wheel hub and steel collar. (a) Von Mises stresses in stresses in collar. (b) Compressive stresses (S11) along the axis of the fibres encircling the primary composite tube (90°).

- Environmental thermal loads and adiabatic effects, influencing material expansion and contraction, are not considered.
- Failure analysis is limited to a first point of failure and the evolution of damage or possible interlaminar and non-linear damage effects are not considered.

4. Structural analysis of the HMC railway axle

A unique aspect of the HMC railway axle is the use of polymer composites in an ultra-high load bearing application, which is further complicated by the condition of fully reversed bending. However, the occurrence of a rotating shaft in 3 or 4 point bending has wide applications and the following generalised methodology is relevant for composite shafts with attached elements such as gears or pulleys using universal metallic collars.

- Step 1: Design the metallic collars so that the wall thickness is sufficient to carry the external load imposed by the interference fit of the wheel onto the collar. The primary composite tube should carry a low level of stress only.
- Step 2: Design the primary composite tube of the axle so that the outer diameter is coincident with the inner diameter of the metallic collar. Specify the ply layup and tube thickness to meet the bending, torsional and horizontal shear stress conditions.
- Step 3: Design the secondary composite tube so that the inner diameter is coincident with the outer diameter of the primary composite tube. Specify the ply layup so that the centre deflection of the axle is minimised.

The analysis is guided by the Tsai-Wu failure criterion [17] which provides a "damage index" at ply level. A damage index of 1.00 or above indicates that an allowable ply strength has been exceeded.

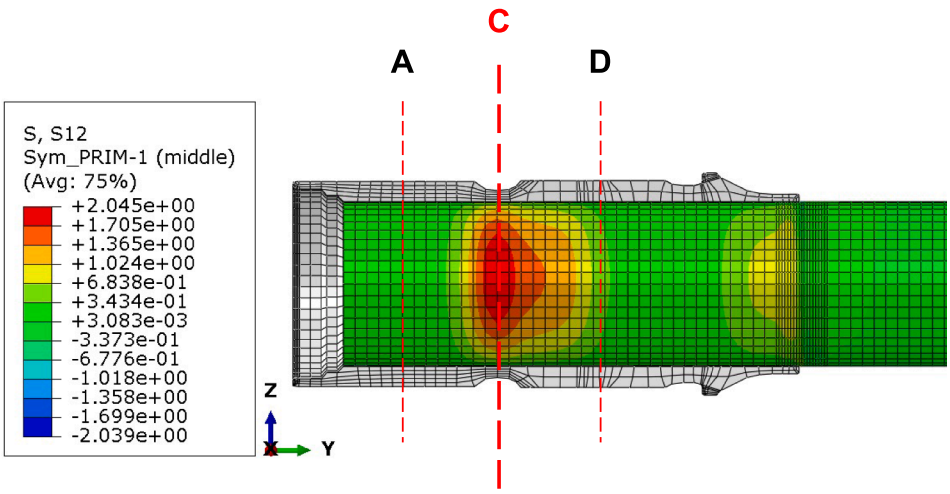

Fig. 8. A cross section through the HMC railway axle at Position *C* showing the maximum value of the horizontal stress in the primary composite tube.

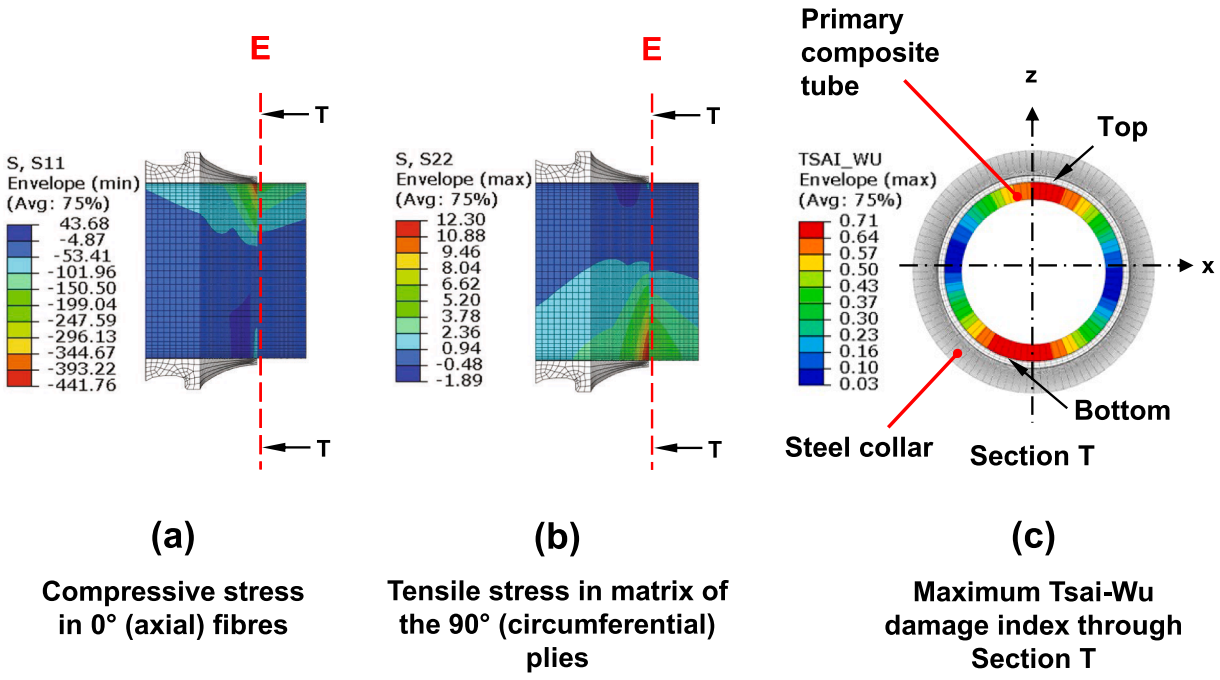

Fig. 9. Stress and damage field in the primary composite tube at Position *E* due to the superimposed masses in motion and braking moments (Note: secondary composite tube omitted for clarity). (a) Compressive S11 (fibre) stress, 0° fibres. (b) Tensile S22 (matrix) stress, 90° fibres. (c) Maximum Tsai-Wu damage index through the cross-sectional *xz*-plane (Section T).

These design sequences are considered in detail in the following sections.

4.1. Step 1: Design of the metallic collars

It is desirable to use the same wheels and bearings on the HMC railway axle as are used on the certificated, hollow steel trailer axle. The axle diameter at the journal is necessarily larger than that of the wheel seat so that the inboard bearing arrangement can be assembled. In addition, the interference fit of the rolling element bearing on to the axle is less than that of the wheel against the axle. Hence, the critical diameter relating to the interference fit is at the running surface (Position *A*). A cross section through the axle is shown in Fig. 6.

The outer diameter of the collar is 177 mm and is aligned with the inner diameter of the wheel hub. The length of the collar is 140 mm. The thickness of the collar is modelled with a nominal dimension of 18.0 mm, allowing for a 0.2 mm adhesive bond line. The collar thickness is dictated by a necessity to maintain an existing geometric feature in the end of the axle.

The primary composite tube has an outer diameter of 142 mm and inner diameter of 115 mm. The wall thickness is 13.5 mm, comprising a balanced layup of 30 plies (see Fig. 4).

4.1.1. Stresses due to external pressure loading

Fig. 7 shows the resultant stress field due to the interference fit (pressure loading) between the wheel hub and the axle collar (Model 1). For this case, moments due to masses in motion (P_x) and braking ($P_x^{'}$ and $P_z^{'}$) are not considered. In addition, the torsional moment,$M_y^{'}$ is not applied.

For the steel collar, the maximum von Mises stress (339 MPa) occurs at the thinned, end feature that overhangs the primary composite tube. In service, a cover is fitted providing support in this region thereby

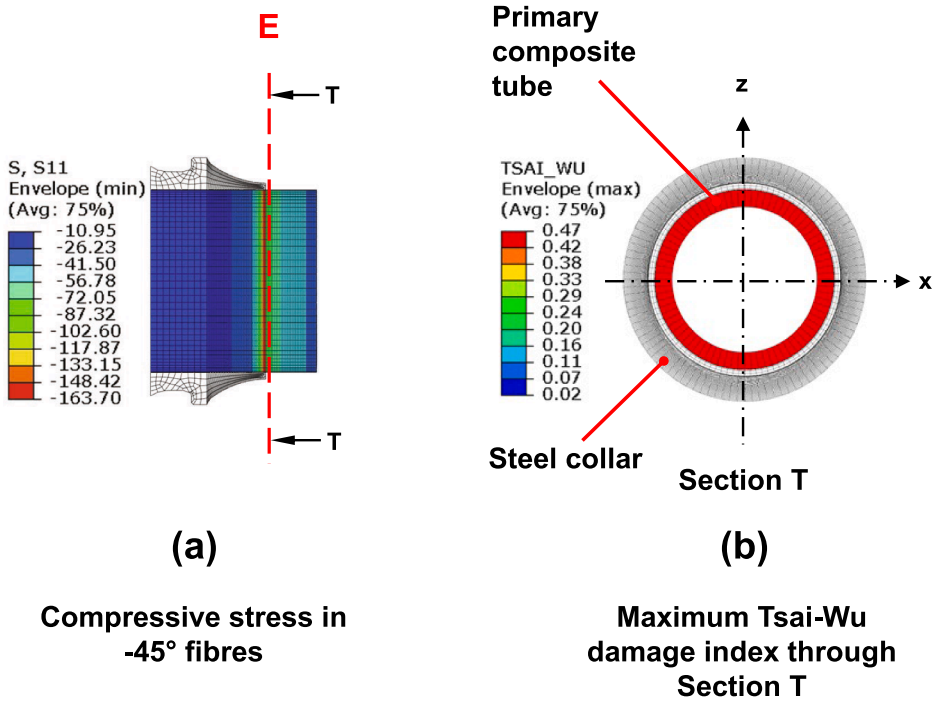

Fig. 10. Stress and damage field in the primary composite tube at Position *E*, due to the torsional moment, $M_y^{'}$ (Note: secondary composite tube omitted for clarity). (a) Compressive S11 (fibre) stress, −45° fibres. (b) Maximum Tsai-Wu damage index through the cross-sectional *xz*-plane (Section T).

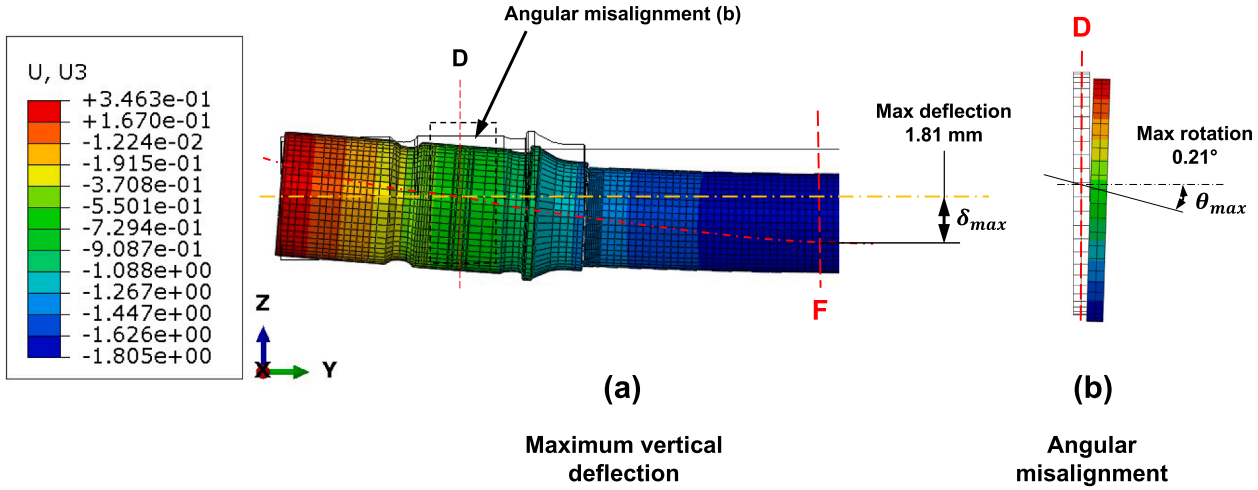

Fig. 11. HMC axle under the combined moments. (a) Vertical displacement field plot (half model) compared against the undeformed state, with a scale factor of 20 applied showing maximum deflection, δ_{max}, at Position *F*. (b) Angular misalignment angle, θ, at Position *D* caused by the axle vertical deflection at the journal seat, with a scale factor 10 applied.

lowering the stress. As is, at Position *A* the stress reduces to approximately 310 MPa which is less than the yield strength of EA1N grade steel (440 MPa). For comparison, this represents a 6% increase over the hollow steel axle. Substitution of a higher yielding metallic collar material, such as Titanium Grade 5 (6Al-4V) as used by Mistry et al [10], would both improve the loading capacity of the collar while reducing the collar mass from 26 kg to 15 kg each.

For the primary composite tube, the dominant stress occurs in the 90° circumferential fibres near the outer surface. These fibres are in axial compression (S11) with a maximum stress of −395 MPa at the end of the tube. This stress reduces to −375 MPa at Position *A*. This is less than the axial compressive strength of the fibre (843 MPa). A maximum Tsai-Wu damage index of 0.3 indicates that failure is unlikely at this position.

4.1.2. Stresses due to shear

Loading due to the masses in motion (P_x) and components due to braking ($P_x^{'}$ and $P_z^{'}$) introduce an internal shear force, *V*, in the HMC axle between the running and loading planes. This produces transverse, or horizontal stress, τ_{horz}, within the HMC axle. For a round, hollow tube, the horizontal stress is maximum at the neutral axis of the cross section [23].

The horizontal stress is highest at Position *C* in the steel collar (42.5 MPa) where the wall thickness is the least (Fig. 8). The same location is chosen to assess the horizontal stress in the primary composite tube

Table 1
Structural performance of the HMC railway axle.

Parameter (Axle Position)	HMC Axle FEA-3D Continuum Element Model	Notes
Mass	74.0 kg Total Collars = 26 kg each Primary composite tube = 14 kg Secondary composite tube = 8 kg	Mass reduction of 63% compared to hollow steel axle.
Interference stresses at wheel seat (A)	Collar = 310 MPa Primary composite tube, $\sigma^{S11,90^{\circ}} = 375$ Mpa (Compressive) Tsai-Wu Index = 0.30 (Model 1)	Hoop wound (90°) fibres under axial compression.
Nominal bending stress, σ_B (F)	99.3 MPa Tsai-Wu Index = 0.18	Primary composite tube
Maximum bending stress, σ_B (E)	$\sigma_B^{S11,0^{\circ}} = 442$ MPa (Compressive) Tsai-Wu Index = 0.66 $\sigma_B^{S22,90^{\circ}} = 12.3$ Mpa (Tensile) Tsai-Wu Index 0.71	Peak stresses due to interaction between steel collar and primary composite tube.
Maximum deflection, δ_{max} (F)	1.71 mm	Hollow steel axle 0.56 mm
Angular misalignment at bearings, θ_{max} (D)	0.21°	Hollow steel axle 0.14°
Back-to-back displacement, ΔL_{BtB} (Rail level)	3.47 mm	Within 6.00 mm tolerance [24]
Maximum horizontal stress, τ_{horiz} (C)	Collar = 42.5 MPa Primary composite tube = 2.05 MPa	
Maximum torsional stress, $\tau_{torsion}$ (E)	$\tau_{torsion}^{S11,-45^{\circ}} = 164$ MPa (Compressive) Tsai-Wu Index = 0.47	
Maximum angular twist, φ (At A from A')	0.32°	
First wheelset bending frequency, ω_1 (Estimated [25])	74 Hz	Hollow steel axle 85 Hz

resulting in a value of 2.05 MPa. As this stress is low, the Tsai-Wu failure criterion is not applied.

In summary, the EA1N grade steel collar with a nominal wall thickness of 17.5 mm can withstand the pressure load (Position *A*) generated by press fitting the wheel onto the axle (310 MPa). At the same location, compressive, circumferential stress is carried into the hoop fibres of the primary composite tube (-375 MPa). The minimal horizontal stresses in both the collar (42.5 MPa) and the primary composite tube (2.05 MPa) are well within the allowable strengths, indicating that failure is unlikely occur in this mode.

4.2. Step 2: Design of the primary composite tube

The design objective is for the primary composite tube to withstand the bending and torsional loading within the limits of the Tsai-Wu failure criterion.

4.2.1. Stresses due to bending

The maximum bending moment arises at the loading plane, Position *D*, and is maintained at a constant value between loading planes. At Position *E*, the collar ends and the diameter of the axle increases due to the additional 13.5 mm thickness of the secondary composite tube. The HMC axle is analysed at Position *E* just before the diameter increases (Fig. 9). The load case includes superposition of all the forces (P_x, $P_x^{'}$ and $P_z^{'}$) that lead to the bending moments, M_x, $M_x^{'}$ and $M_z^{'}$. Of importance is that as the axle rotates, the configuration changes and the axle is subject to fully reversed bending for each cycle. The torsional moment,$M_y^{'}$ is not applied in this case.

The maximum stress and damage index, shown in Fig. 9, is due to the localised bending stress, σ_B, at Position *E* in the primary composite tube where the cross section is minimal.

This causes a dominant compressive, S11 fibre stress (-442 MPa) in the 0° plies nearest the outer surface, orientated at the "Top" of the tube. These fibres are aligned with the global *y*-axis of the railway axle. Furthermore, a tensile S22 matrix stress (12.4 MPa) in the 90° plies nearest the outer surface at the "Bottom" of the tube arises. These are the hoop fibres being loaded transversely in the direction of the global *y*-axis. The relative S11 and S22 stress results produce Tsai-Wu damage index values of 0.66 and 0.71, respectively.

The average through thickness stress in the stacking direction at Position *E* is 10.7 MPa. This is caused by the penetration compliance of the collar to the top side of the primary composite tube. A refinement study at Position *E* showed little variation in the stress field with a finer mesh size of 1 mm.

4.2.2. Stresses due to torsion

Application of the moment, $M_y^{'}$, to the HMC railway axle at Position *D*' produces torsional stress, $\tau_{torsion}$, across the axle. The bending moments, M_x, $M_x^{'}$ and $M_z^{'}$ are not applied in this load case.

The maximum torsional stress occurs at Position *E*, where the cross-sectional diameter is the least. Fig. 10 shows the stress and damage field in the primary composite tube. The dominate compressive, S11 fibre stress (−164 MPa) is in the −45° plies nearest the surface (Fig. 10a), Transverse to the −45° (S22) a tensile stress develops in the matrix with a maximum of 3.28 MPa. The corresponding Tsai-Wu damage index is 0.47 (Fig. 10b).

The torque, $M_y^{'}$, produces twist in the axle, φ. The maximum angle of twist occurs at Position *A* under the scenario of a seized wheel at Position $A^{'}$ and has a value of 0.32°.

In summary, the primary composite tube with a nominal wall thickness of 13.5 mm can withstand the bending and torsional moment components of the loading. Traditionally, the axle would be assessed at the centre of the axle (Position *F*) where the bending deflection is greatest. Here, the nominal stress is 99.3 MPa, with a corresponding Tsai-Wu damage index of 0.18. However, at the reduced cross-section (Position *E*), the combination of a peak stress and the potential for collar penetration to the OD of the composite tube under bending affects the distributed stress at this position. While the Tsai-Wu criterion is not exceeded (maximum of 0.71), engineering of the collar to primary composite tube joint is advisable. The torsional stress and associated twisting around the *y*-axis is less severe (maximum Tsai-Wu damage index of 0.47) as anticipated by the Standard [12].

4.3. Step 3: Design of the secondary composite tube

The main function of the secondary composite tube is to permit stiffness tailoring of the HMC railway axle, controlling deflection. Altering the ply orientations and laminate thickness affects the flexural rigidity of the axle. In this way the static and dynamic properties of the axle can be tuned to meet the performance requirements. In addition, the secondary composite tube improves the structural capacity of the primary composite tube.

4.3.1. Deflection due to bending

As the HMC axle is under four-point bending, maximum deflection occurs at the centre of the axle, Position *F* (Fig. 11a). The torsional moment,$M_y^{'}$ is not applied in this case. Associated with the deflection of

the axle is the angular misalignment at the journal shown in Fig. 11b. The axle is oriented to show the deflection as downward vertical bending in the section of the HMC axle where the primary composite tube is reinforced by the secondary composite tube. The greatest deflection, δ_{max}, is 1.71 mm.

The deflection also increases the back-to-back distance by ΔL_{BtB} between the wheel flanges at rail level. For the HMC railway axle, $\Delta L_{BtB} = 3.47$ mm which is within the accepted tolerance of 6 mm [24].

An indication of the angular misalignment imposed on the tapered roller bearings is described by the degree of rotation, θ, (Fig. 11b) calculated from the rotational degree of freedom around the x-axis at the surface nodes of the journal seat for Position D. This maximum rotation, θ_{max}, is equivalent to 0.21° and compares with a value of 0.14° for the hollow steel axle. If necessary, the internal clearance of the bearing could be increased, or a self-aligning bearing system could be specified.

4.3.2. First bending frequency

The first bending frequency, ω_1, of the wheelset comprising the HMC railway axle is estimated at 74 Hz using a simplified method described by Peng et al [25]. For comparison, a value of 85 Hz is obtained for the hollow steel axle using the same technique. A refined analysis is required as a wheelset bending frequency in the range of 90–110 Hz is prescribed and what the hollow steel axle is expected to achieve [16].

In summary, the secondary composite tube with a nominal wall thickness of 13.5 mm constrains the maximum deflection of the axle to 1.71 mm with a back-to-back distance of 3.47 mm. The increase in axial misalignment at the journals requires further investigation if a standard tapered rolling element bearing is to be used. The greatest stress in the secondary composite tube is less than 185 MPa (S11) and 6 MPa (S22) for symmetrical bending with a Tsai-Wu damage index of 0.3. Further stiffening of the axle is possible by adding additional layers of reinforcement to the secondary composite tube with a mass penalty of approximately 0.30 kg per layer. This may be considered for tuning the wheelset bending frequency.

4.4. Summary of the structural performance of the HMC railway axle

The structural performance parameters for the HMC railway axle (Fig. 4) obtained by the 3D continuum element model within Section 4 are summarised in Table 1 (Model 2 except where noted).

5. Discussion

A modern, steel railway axle is a complex, safety critical component which has benefited from many years of in-service use with complementary scrutiny of performance. The scope of this paper is restricted primarily to the function of the axle as a structural member. Other important functions of the axle relating to, for example, fatigue reliability, damage tolerance, electrical grounding, even fire performance will require fuller consideration to raise the fidelity of the design to a high technical readiness level. Here, a preliminary structural analysis of a lightweight, HMC (hybrid metallic composite) railway axle has been presented using a FE model. This model first provided a verification of previous design by Mistry et al. [5] and allowed refinements to be made. In addition, stress concentrations, particularly at the collar ends were analysed using the FE model. The total mass of the axle is 74.0 kg, a reduction of 63% compared to an equivalent hollow steel axle. The FE model was used to analyse the interference fit of the collars as well as bending and torsional response of the HMC axle. The structural performance of the HMC railway axle is summarized in Table 1.

Aligned with the design approach presented by Mistry et al [10], the thickness of the metallic collars are specified first to withstand the pressure of the interference fit of the wheel without damage propagation through the collar to the primary composite tube. EAN1 steel at a nominal thickness of 18 mm was used for this purpose. The stress in the collar is 310 MPa, resulting in a circumferential compressive stress on the hoop wound (90°) fibres of 375 MPa and a Tsai-Wu damage index of 0.30. While the stress in the collar is less than the yield strength of the material, the Standard BS 8535 [12] specifies a more stringent strength allowable in the wheel seat region. The steel collars also mitigate horizontal stresses within the primary composite tube in the non-uniform bending region between the running surfaces and the loading planes. A horizontal stress of 2.05 MPa develops in the primary composite tube at the smallest overall radius indicating that failure in this mode is not likely.

The second step in the analysis was to establish the thickness of the primary composite tube. A value of 13.5 mm was determined to withstand the bending and torsional loading under a 50% strength reduction due to fatigue loading (10^7 cycles). The nominal bending stress at the middle of the tube (Position F) is 99.3 MPa with a Tsai-Wu damage index of 0.13 indicating a low likelihood of failure. The occurrence of a high peak stress in the tube at the in-board end of the collar (Position E) presents the greatest challenge to the design. Here, the axial fibres (0°) undergo a compressive stress of 442 MPa (Tsai-Wu damage index of 0.66) while the hoop wound fibres (90°) sustain a transverse tensile stress of 12.3 MPa (Tsai-Wu damage index of 0.71). Engineering of the collar joint at this position is necessary to reduce these stresses. While bending is the predominant load case, the effect of torsion at Position E is also presented. Here the −45° fibres exhibit a compressive (buckling) stress of 164 MPa with a Tsai-Wu damage index of 0.47.

The final step in the analysis is to specify the orientation and thickness of the secondary composite tube. The purpose of this tube is to permit adjustment of the flexural rigidity of the axle and thereby influence the bending deflection and the onset of shaft whirl. The maximum deflection of the HMC axle is 1.71 mm at the centre compared to 0.56 mm for the hollow steel axle. This results in a back-to-back wheel deflection of 3.58 mm which is within the 6 mm tolerance for this parameter [24]. The angular misalignment at the bearings is limited to 0.21° compared to 0.14° for the hollow steel axle. As the loading in the FE model has been applied at a point rather than distributed, further analysis of the journal region is necessary before recommending either an increase in internal clearance for the bearing or a change to a self-aligning bearing system. The first wheelset bending frequency is estimated at 74 Hz and is comparable to that for the hollow steel axle at 85 Hz [25], although both are below the accepted frequency range of 90–110 Hz [16] indicating that a more rigorous analysis of shaft whirl is necessary.

While the design methodology has been used for a railway axle, the approach is generic and could be used for the design of any composite shaft using metallic collars for the attachment of shaft elements. Notable applications include shafts within an aero engine gearbox where the mass reduction translates to significant fuel savings. Adoption for a wind turbine main shaft would ease handling during installation with potential stability gains afforded by the lower mass at the top of the mast. Finally, a new generation of machines for space exploration are envisaged where low mass shafts will contribute to a lighter launch weight.

A clear area for further study is in the design of the metallic collars and the joint with the primary composite tube. The high peak stress where the collar impinges on the surface of primary tube is within the limits of the Tsai-Wu criterion for the static loading case. However, efforts to reduce this should be addressed. The adhesive bond between the collar and the primary composite tube is an area of future work. While initial laminate analysis has been adopted in the FEA of this HMC railway axle, full optimisation of the laminate has not been undertaken. A second area of future work is the development of a computational design tool that permits rapid assessment of ply failure under loading at discrete, critical sections of this axle. This would allow the ply stacking sequence to be optimised prior to undertaking an intensive FEA study.

6. Conclusion

This work provides a structural analysis of a lightweight hybrid

metallic-composite (HMC) railway axle, first proposed by Mistry et al [10]. That manuscript proposed a mechanics of materials approach using a netting analysis to establish fibre weightings. The FEA model in this work confirmed that analysis and was further extended to areas on the HMC railway axle with stress concentrations. The resulting mass of 74 kg represents a 63% reduction to the equivalent hollow steel axle. A finite element analysis was performed using the general design approach set out in the Standard BS 8535 being followed. While a new Standard will be required for the HMC railway axle, the load cases within BS 8535 are expected to apply irrespective of the material solution used.

The axle comprises a full length, primary composite tube (OD = 142 mm, ID = 115 mm) manufactured from a high modulus carbon fibre, epoxy prepreg to withstand the bending and torsional loadings as provided by Lucchini R. S. A secondary composite tube (OD = 169 mm, ID = 142 mm), using the same prepreg material, is applied to the central region of the axle between the loading planes and controls the flexural rigidity of the axle. Collars made from EA1N grade steel with the exterior profile (nominal OD = 177 mm) matching a standard, hollow steel axle and an ID = 142 mm are bonded onto either end of the primary composite tube. The collars are designed to withstand the compressive, interference fit of the wheel onto the collar without damaging the primary composite tube.

The nominal bending stress at the centre of the axle is 99.3 MPa (Tsai-Wu damage index of 0.18). Peak bending stresses occurs within the primary composite tube inboard of the collar. Here, the hoop (90°) fibres are loaded transversely resulting in a Tsai-Wu damage index of 0.71 at the condition of 10^7 bending cycles. Although meeting the failure criterion, this joint requires further analytical design. The principle of attaching a metallic collar with a hard outer surface to a composite shaft represents a generic solution for fastening, application dependent shaft elements (for example, brake discs, gears, pulleys or flywheels).

Shear stress due to torsion (Tsai-Wu damage index of 0.42) as well as the horizontal shear stress (2.05 MPa) between the running surfaces and loading planes indicate that failure by these mechanisms is unlikely.

The maximum deflection at the centre of the axle is 1.71 mm, with an increase in the back-to-back wheel dimension being held within tolerance at 3.47 mm. However, the angular misalignment is 0.21° at the bearings requires further analysis if double row tapered bearings are to be used. Furthermore, a rigorous assess of the wheelset first bending frequency is recommended to ensure Standard compliance.

The methodology used for the design to the HMC railway axle is generic and could be applied to any composite shaft with elements attached using universal metallic collars. Conceivable applications include the shafts within an aero engine gearbox, the main shaft of a wind turbine or any shaft driven machine for space exploration.

Structurally, further understanding of the high cycle (10^9) fatigue properties of the composite under fully reversed bending and the failure mode of the axle is necessary to bring this study to a higher technology readiness level. Implementation of a rapid, CLT numerical solver would allow the designer to optimise the ply stacking sequence prior to commitment to an FEA solution. This is recommended as an area of additional future work.

Author contribution

M.S. Johnson: Methodology, Writing – original draft. **R. Evans:** FEA and Writing. **P.J. Mistry:** Writing – original draft, Writing – review & editing. **S. Li:** Supervision, Writing – review & editing. **S. Bruni:** Project administration, Writing – review & editing. **A. Bernasconi:** Project administration, Writing – review & editing. **S. Cervello:** Project administration, Writing – review & editing.

Declaration of Competing Interest

The authors declare that they have no known competing financial interests or personal relationships that could have appeared to influence the work reported in this paper.

Acknowledgements

This work was conducted as part of Work Package 3 of the NEXTGEAR Project, S2R-OC-IP1-02-2019 [Grant number: 881803], which is ascribed under the Shift2Rail Program funded by the EU Horizon 2020 research and innovation programme.

The third author would like to acknowledge the funding support of the Engineering and Physical Sciences Research Council through the: EPSRC Future Composites Manufacturing Research Hub [Grant number: EP/P006701/1] and EPSRC Doctoral Prize Fellowship [Grant number: EP/T517902/1].

***Data** availability*

The raw/processed data required to reproduce these findings cannot be shared at this time as the data also forms part of an ongoing study.

Appendix

The following tables include material properties used as input to the FEA models. These include the EA1N grade steel used for the collars (Table A1), ER7 grade steel for the wheel hub (Table A2), carbon fibre reinforced epoxy prepreg (Gurit-UCHM450 SE 84LV) used for the primary and secondary composite tubes (Table A3) and the adhesive (3M™-Scotch-Weld 9323B/A Two Part Structural Adhesive) (Table A4).

Table A1
Mechanical properties of AISI 1030, 0.3% C steel, normalised, representing EA1N grade steel for the collars [22].

Mechanical property	Symbol	Value	Unit
Modulus of elasticity	$E_{St,EA1N}$	200	GPa
Shear modulus	$G_{St,EA1N} = \frac{E_{St,EA1N}}{2(1+\upsilon_{St,EA1N})}$	77.8	GPa
Yield strength	$\sigma_{St,EA1N,y}$	440	MPa
Poisson's ratio	$\upsilon_{St,EA1N}$	0.285	–
Density	$\rho_{St,EA1N}$	7850	kg/m^3
Average fatigue strength at 10^7 cycles	$\sigma_{St,EA1N,fat10^7}$	270	MPa

Table A2
Mechanical properties of AISI 1050, 0.5% C steel, normalised, representing ER7 grade steel for the wheel [22].

Mechanical property	Symbol	Value	Unit
Modulus of elasticity	$E_{St,ER7}$	215	GPa
Shear modulus	$G_{St,ER7} = \frac{E_{St,ER7}}{2(1+\upsilon_{St,ER7})}$	82.5	GPa
Yield strength	$\sigma_{St,ER7,y}$	580	MPa
Poisson's ratio	$\upsilon_{St,ER7}$	0.295	–
Density	$\rho_{St,ER7}$	7850	kg/m^3
Average fatigue strength at 10^7 cycles	$\sigma_{St,ER7,fat10^7}$	350	MPa

Table A3
Mechanical properties of Gurit UCHM450 SE 84LV unidirectional (0°) prepreg for the primary and secondary composite tubes (Source: Gurit).

Mechanical property	Symbol	Value	Unit
Fibre volume fraction	v_f	56	%
Ply thickness	t_{ply}	0.45	mm
Ply weight	W_{ply}	683	g/m^2
Density	ρ	1498	kg/m^3
Longitudinal tensile modulus	$E_{11,t}$	208.26	GPa
Longitudinal tensile strength	$\sigma_{11,t}$	1562	MPa
Longitudinal tensile fatigue strength at 10^7 cycles (estimated)	$\sigma_{11,t,fat10^7}$	781	MPa
Longitudinal compressive modulus	$E_{11,c}$	187.43	GPa
Longitudinal compressive strength	$\sigma_{11,c}$	843.40	MPa
Longitudinal compressive fatigue strength at 10^7 cycles (estimated)	$\sigma_{11,c,fat10^7}$	421.7	MPa
Transverse tensile modulus	$E_{22,t}$	6.39	GPa
Transverse tensile strength	$\sigma_{22,t}$	28.80	MPa
Transverse compressive modulus	$E_{22,c}$	6.39	GPa
Transverse compressive strength	$\sigma_{22,c}$	83.1	MPa
Interlaminar shear modulus	E_{13}	4.31	GPa
Interlaminar shear strength	σ_{13}	64.70	MPa
In-plane shear modulus	E_{12}	4.31	GPa
In-plane shear strength (estimated)	σ_{12}	64.70	MPa
Poisson's ratio – longitudinal strain	v_{12}	0.337	–

Table A4
Mechanical properties of 3 M™ Scotch-Weld 9323B/A Two Part Structural Adhesive for the bonding of collars to primary composite tube (Source: 3 M).

Mechanical property	Symbol	Value	Unit
Modulus of elasticity	$E_{adhesive}$	2.133	GPa
Poisson's ratio	$v_{adhesive}$	0.33	–

References

[1] OECD. Passenger transport (indicator), https://data.oecd.org/transport/passenger-transport.htm, Access Date 23/05/2021, doi: 10.1787/463da4d1-en. 2021.
[2] ERRAC. Rail 2050 Vision: Rail-The backbone of Europe's mobility, 122017_ERRAC-RAIL-2050.pdf. 2017.
[3] Iwnicki S, Spiryagin M, Cole M, McSweeney T. Handbook of Railway Vehicle Dynamics. 2nd ed: CRC Press; 2019.
[4] Wu SC, Liu YX, Li CH, Kang GZ, Liang SL. On the fatigue performance and residual life of intercity railway axles with inside axle boxes. Eng Fract Mech 2018;197:176–91.
[5] Regazzi D, Cantini S, Cervello S, Foletti S, Pourheidar A, Beretta S. Improving fatigue resistance of railway axles by cold rolling: Process optimisation and new experimental evidences. Int J Fatigue 2020;137:105603.
[6] Mistry PJ, Johnson MS. Lightweighting of railway axles for the reduction of unsprung mass and track access charges. Proceedings of the Institution of Mechanical Engineers, Part F: Journal of Rail and Rapid Transit. 2019;234:958-68.
[7] Beretta S, Regazzi D. Probabilistic fatigue assessment for railway axles and derivation of a simple format for damage calculations. Int J Fatigue 2016;86:13–23.
[8] Makino T, Sakai H, Kozuka C, Yamazaki Y, Yamamoto M, Minoshima K. Overview of fatigue damage evaluation rule for railway axles in Japan and fatigue property of railway axle made of medium carbon steel. Int J Fatigue 2020;132:105361.
[9] Gao J-W, Dai G-Z, Li Q-Z, Zhang M-N, Zhu S-P, Correia JAFO, et al. Fatigue assessment of EA4T railway axles under artificial surface damage. Int J Fatigue 2021;146:106157.
[10] Mistry PJ, Johnson MS, Li S, Bruni S, Bernasconi A. Parametric sizing study for the design of a lightweight composite railway axle. Compos Struct 2021;267:113851.
[11] Batchelor J. Use of fibre reinforced composites in modern railway vehicles. Mater Des 1981;2(4):172–82.
[12] British Standards Institution. BS 8535:2011-Railway applications–Wheelsets and bogies–Powered and non-powered axles with inboard bearings–Design method. London, England, UK: BSI; 2011.
[13] Hu Y, Yang Mo, Zhang J, Song C, Hong T. Effect of stacking sequence on the torsional stiffness of the composite drive shaft. Adv Compos Mater 2017;26(6):537–52.
[14] Tataroğlu S, Ok E, Kaya S, Şen A, Doğan VZ, Mecitoğlu Z, et al. Design and manufacturing of a composite drive shaft. Key Eng Mater 2016;706:73–7.
[15] Montagnier O, Hochard C. Optimisation of hybrid high-modulus/high-strength carbon fibre reinforced plastic composite drive shafts. Mater Des 2013;46:88–100.
[16] Mistry PJ, Johnson MS, Jones IA, Bernasconi A, Bruni S, Carboni M, et al. NEXTGEAR D3.1–Analysis of the state of the art for composite materials suitable for rail wheelsets and related manufacturing processes. 2020.
[17] Campbell FC. Structural Composite Materials. 1st ed. Materials Park, Ohio, USA: ASM International; 2010.
[18] Python software version 3.10.0. Python Software Foundation. Available at http://www.python.org; 2021.
[19] Jones RM. Mechanics of Composite Materials. 2nd ed. Washington, D.C. USA: Taylor & Francis, 1998.
[20] MATLAB. R2020a Update 4 (9.8.0.1417392) ed: The MathWorks Inc., Natick, Massachusetts, USA; 2020.
[21] British Standards Institution. BS EN 13260:2009+A1:2010-Railway applications-Wheelsets and bogies-Wheelsets-Product requirements. London, England, UK: BSI; 2010.
[22] EduPack CES. software version 18.1.1. Cambridge, UK: Granta Design Limited; 2018.
[23] Goodno BJ. Timoshenko-Mechanics of materials. 7th ed., SI / James M. Gere, Barry J. Goodno. ed. Boston, Mass.: Boston, Mass. : Cengage Learning, 2009.
[24] Commission Regulation (EU), Technical Specification of interoperability "Loc & Pass", in TSI Loc & Pas 1302/2014. 2014.
[25] Peng Bo, Iwnicki S, Shackleton P, Crosbee D, Zhao Y. The influence of wheelset flexibility on polygonal wear of locomotive wheels. Wear 2019;432-433:102917.